ChemComm
Chemical Communications

Accepted Manuscript

This article can be cited before page numbers have been issued, to do this please use: G. Fan, H. Zhao, L. Ma, Y. Lu and X. Luo, *Chem. Commun.*, 2020, DOI: 10.1039/C9CC08472J.

ROYAL SOCIETY OF CHEMISTRY

rsc.li/chemcomm

ROYAL SOCIETY OF CHEMISTRY
View Article Online
DOI: 10.1039/C9CC08472J

Journal Name

COMMUNICATION

Distance-triggered signaling on-off mechanism by plasmonic Au nanoparticles: toward advanced photocathodic DNA bioanalysis

Received 00th January 20xx,
Accepted 00th January 20xx

DOI: 10.1039/x0xx00000x

www.rsc.org/

Gao-Chao Fan[a], Huan Zhao[a], Linzheng Ma[ab], Yanwei Lu[a] and Xiliang Luo*[a]

An efficient signaling on-off mechanism was first proposed by integrating exciton–plasmon coupling and exciton energy transfer into cathodic PEC bioassay. This signaling on-off mechanism has endowed the cathodic PEC biosensor with powerful capability to ultrasensitive and specific detection of target DNA.

With ever-increasing requirement for sensitive, selective, facile and rapid detection of specific DNA sequences, sustained and great efforts have been made by the researchers to explore powerful techniques with advanced signaling mechanisms.[1,2] Owning to the distinct merits such as high sensitivity, low background signal, easy operation and high throughput, photoelectrochemical (PEC) technique for DNA bioanalysis has shown its bright prospect and attracted increasing attention.[3-5] It has been demonstrated that cathodic PEC biosensors, which are built on photocathode and use p-type photoactive material as substrate, have shown huge potential to resist interference from reductive species, and thus stimulated strong research interests.[6-9] Despite this, the exploration of high-performance cathodic PEC biosensors is still in its infancy. As a result, advanced signaling mechanism that with superior capability for photocathodic bioanalysis is beyond a doubt highly desirable.

So far, for cathodic PEC sensors, the signaling mechanisms such as sensitization effect, energy transfer, steric-hindrance, and enzymatic reaction have been utilized alone to trigger or enhance the photocurrent signal for various targets. Thereinto, energy transfer is an effective strategy to decrease the photocurrent signal for building DNA related biosensors,[10,11] which is operated upon the spectral overlap combining with proper distance (around 10 nm) between energy donors and acceptors. The energy donors are usually semiconductor quantum dots (QDs), while the energy acceptors are metallic nanoparticles (NPs). Similar with energy transfer, exciton–plasmon coupling can also happen between semiconductor QDs and metallic NPs, but close contact of them is necessary.[12,13] Exciton–plasmon coupling is known as a special interaction between exciton-polaritons (in semiconductor) and plasmon-polaritons (in metallic NPs), which allows excited electrons to smoothly transfer between conduction band of QDs and surface plasma states of metallic NPs.[13-14] This phenomenon can evidently increase the lifetime of the excited electrons, and hence effectively inhibit the charge (electron-hole pair) recombination.[13-15] Accordingly, integrating signaling mechanism of exciton–plasmon coupling into cathodic PEC biosensors can evidently enhance the cathodic photocurrent, while which has not been reported yet. As exciton–plasmon coupling and energy transfer have opposite effects to cathodic photocurrent, if possible, a joint signal amplification could be produced by regulating the distance between semiconductor QDs and metallic NPs to control the occurrence of exciton–plasmon coupling and energy transfer, which would contribute significantly to ultrasensitive photocathodic detection.

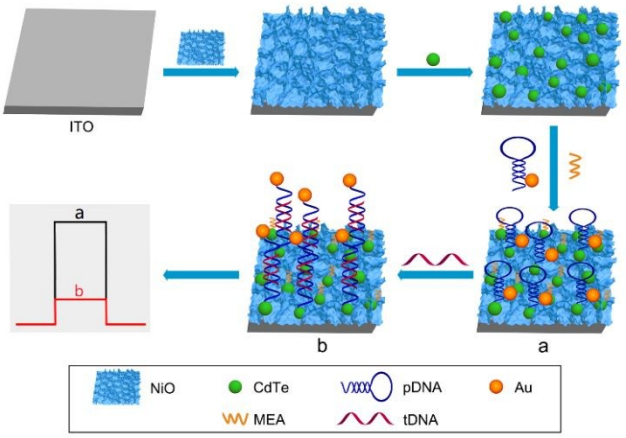

Scheme 1. Cathodic PEC DNA bioassay based on proposed signaling on-off mechanism.

[a] *Key Laboratory of Optic-electric Sensing and Analytical Chemistry for Life Science, MOE; College of Chemistry and Molecular Engineering, Qingdao University of Science and Technology, Qingdao 266042, China. E-mail: xiliangluo@qust.edu.cn*
[b] *College of Chemical and Environmental Engineering, Shandong University of Science and Technology, Qingdao 266590, China*

Electronic Supplementary Information (ESI) available: Experimental details; XPS of photocathode; UV-vis DRS of photocathode; characterization of AuNPs-pDNA; optical imaging of biosensor; optimal condition of biosensor; selectivity, stability repeatability and feasibility. See DOI: 10.1039/x0xx00000x

Herein, inspired by the situation above, an advanced signaling on-off mechanism regulated by plasmonic AuNPs was proposed to build an ingenious and efficient cathodic PEC DNA bioassay, as illustrated in Scheme 1. The DNA sequence of BCR/ABL fusion gene (type b3a2) associated with chronic myelogenous leukemia (CML) was served as the target DNA (tDNA). Experimentally, three-dimensional (3D) NiO nanofilm was first fabricated on an indium tin oxide (ITO) substrate by hydrothermal reaction and then assembled with CdTe QDs via layer-by-layer method to prepare the CdTe/NiO photocathode. AuNPs as signaling labels were covalently bound on the terminal of hairpin-structured probe DNA (pDNA) to form AuNPs-pDNA conjugates. After the CdTe/NiO photocathode was immobilized with AuNPs-pDNA conjugates and then blocked with monoethanolamine (MEA), the cathodic PEC biosensor was built. The tDNA was detected by the dramatic photocurrent decrease produced from conformation change of the pDNA after the specific DNA hybridization, which brought about disappeared exciton–plasmon coupling concurrent with generated exciton energy transfer. This superior signaling on-off mechanism has endowed the cathodic PEC biosensor with powerful capability to ultrasensitive and specific detection of tDNA.

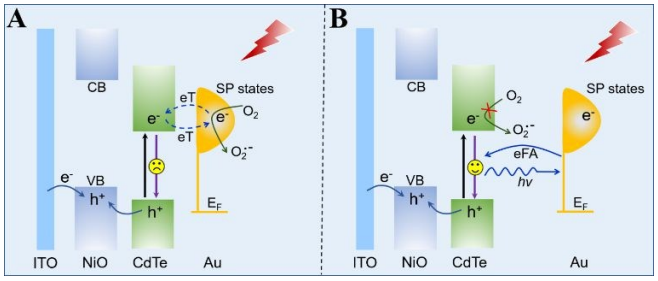

Scheme 2. PEC signaling on-off mechanism for photocathodic DNA bioanalysis. **Note**: eT, eFA, and *hv* in the scheme stand for electron transfer, electric field action, and emission energy, respectively.

In the proposal, the CdTe/NiO photocathode was used as matrix to immobilize pDNA with plasmonic AuNPs on the terminal. The different roles of plasmonic AuNPs labeling were triggered by conformation change of pDNA after hybridization with tDNA. The PEC signaling on-off mechanism for photocathodic DNA bioanalysis was illustrated in Scheme 2. NiO is a typical p-type wide-band-gap semiconductor (E_g=3.6–4.0 eV) with good stability, which shows a promising candidate for photocathode substrate.[16,17] Yet, as NiO mainly harvests the ultraviolet light, just a very weak cathodic photocurrent could be obtained under visible-light irradiation. CdTe is a familiar narrow band-gap semiconductor with E_g value of 1.5 eV, which renders CdTe an ideal material for visible light absorption.[18,19] Coupling CdTe with NiO can effectively harvest the visible light, and the stepwise band edges of NiO and CdTe benefits the charge separation. As a result, the CdTe/NiO photocathode had an obvious cathodic photocurrent.

In the absence of tDNA, the labels of plasmonic AuNPs were in close contact with the CdTe/NiO photocathode. At this time, as shown in Scheme 2A, the exciton–plasmon coupling formed between photogenerated electrons within conduction band (CB) of the CdTe QDs and hot electrons in surface plasma (SP) states of the plasmonic AuNPs.[13,14] This exciton–plasmon coupling induced resonance is typically known for increasing the lifetime of the electrons in the excited state, and hereby, it evidently inhibited the charge recombination.[13-15] Accordingly, the cathodic photocurrent of the AuNPs-pDNA modified CdTe/NiO photocathode obviously enhanced compared with pure pDNA modified CdTe/NiO photocathode (signal on).

In the presence of tDNA, the labels of plasmonic AuNPs left from the electrode surface and kept a certain distance with CdTe/NiO photocathode. Under this situation, as shown in Scheme 2B, the exciton–plasmon coupling between the CdTe QDs and plasmonic AuNPs disappeared, and conversely, the exciton energy transfer between them happened. Because of the overlap between emission band of the CdTe QDs and SPR absorption region of the AuNPs, the emission generated by charge recombination of the CdTe QDs would induce SPR absorption of the AuNPs with the formation of a local electric field,[20,21] which further increased the charge recombination ratio in the CdTe QDs and hereby decreased the cathodic photocurrent (signal off). Benefitting from disappearance of the exciton–plasmon coupling concurrent with generation of the exciton energy transfer, the cathodic PEC signal for tDNA detection would be very conspicuous. Compared with traditionally reported signal-on or signal-off mechanism, the proposed signaling on-off mechanism had superior capability for signal amplification, and hence the ultrasensitive detection of target could be realized.

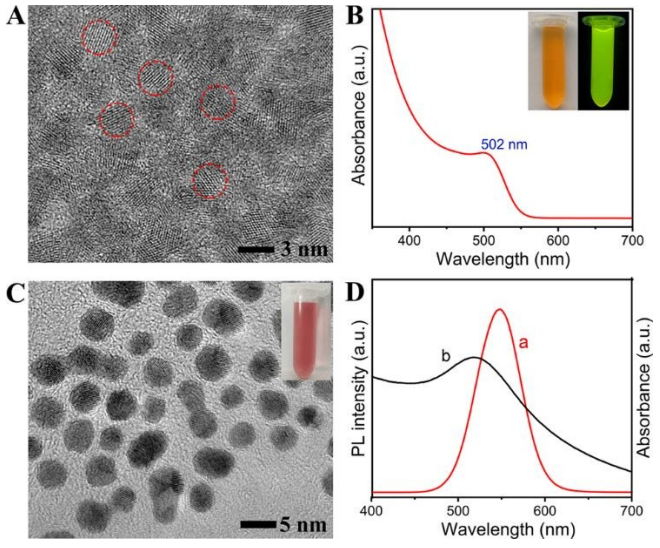

Fig. 1. (A) HRTEM image and (B) UV-vis absorption spectrum of the CdTe QDs; (C) HRTEM images of the AuNPs; (D) PL emission spectrum of (a) the CdTe QDs and (b) absorption spectrum of the AuNPs. Inset in B and C: photographs of CdTe QDs solution (under white light and UV-lamp) and AuNPs solution (under white light).

The synthesized CdTe QDs sample was first characterized by high-resolution transmission electron microscopy (HRTEM) image, as shown in Fig. 1A. The lattice fringes of the QDs were clearly shown in the HRTEM image and their average size of

2.8 nm was obtained from the clear outlines of theses QDs. Fig. 1B exhibits UV–visible (UV-vis) absorption spectrum of the CdTe QDs, and a relatively broad absorption region to 560 nm with an obvious absorption peak at 502 nm could be found in the spectrum. The insets in Fig. 1B shows photographs of the CdTe QDs solution. The bright-green fluorescence indicated high quality of the QDs. Fig. 1C shows HRTEM image of the synthesized AuNPs, and the average size of about 4.5 nm was obtained from their clear outlines and lattice fringes. For effective exciton energy transfer, the spectral overlap is necessary. As shown in Fig. 1D, the CdTe QDs exhibited a sharp photoluminescence (PL) emission peak at 547 nm (curve a), while AuNPs showed an evident plasmon absorption peak at about 518 nm (curve b). It is noted that the emission band of the CdTe QDs had a considerable overlap with the SPR absorption region of the AuNPs, which was very beneficial to the inducement of SPR effect of the AuNPs.

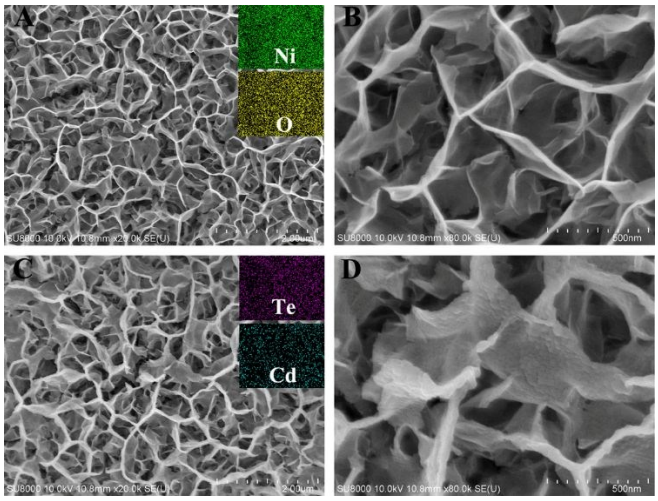

Fig. 2. (A, B) SEM images of the NiO film modified ITO electrode with (A) low and (B) high magnification; (C, D) SEM images of the hybrid CdTe/NiO film modified ITO electrode with (C) low and (D) high magnification. Inset in A and C: elemental mapping analysis of (Ni, O) and (Te, Cd).

Fig. 2A and 2B show scanning electron microscopy (SEM) images of NiO film modified ITO electrode with low and high magnifications. As depicted in Fig. 2A, the prepared NiO film was composed of abundant interconnected nanoflakes and appeared a highly crossed 3D porous nanostructure. It can be observed in Fig. 2B that these nanoflakes was smooth with about 12 nm in thickness and micron size in lateral dimension. The 3D porous nanostructure of the NiO film could offer a huge surface area to the subsequently modified CdTe QDs, which was conducive to the efficient light absorption and charge exchange at the electrode interface. Fig. 2C and 2D then reveal SEM images of the hybrid CdTe/NiO film with low and high magnifications. It can be clearly observed that the guests of CdTe QDs were evenly coated onto the surface of the 3D porous NiO film (Fig. 2C), and the previous NiO nanoflakes became rough and thick (Fig. 2D). The elemental mapping analysis in the insets of Fig. 2A and 2C also suggested the modification of CdTe QDs on the NiO nanoflakes. Besides, the X-ray photoelectron spectroscopy (XPS) further confirmed successful fabrication of the CdTe/NiO photocathode (Fig. S1).

The stepwise building of the DNA biosensor was inspected by photocurrent response, as shown in Fig. 3A. The NiO layer modified ITO electrode showed a small cathodic photocurrent (curve a) owning to intrinsic large band-gap and low visible-light adsorption of NiO substrate. After CdTe QDs modification, the CdTe/NiO photocathode exhibited a significantly increased cathodic photocurrent (curve b), because the CdTe QDs with narrow band-gap obviously extended the absorption range (Fig. S2) and as a result presented a conspicuous sensitization effect to NiO nanofilm. To verify positive role of the AuNPs labeling in cathodic photocurrent enhancement, pure pDNA was used as a reference of the AuNPs-pDNA conjugate. After pure pDNA anchoring on the photocathode, an obvious decrease in the cathodic photocurrent could be observed (curve c), which might be attributed to weak charge transfer of the pDNA. While AuNPs-pDNA conjugates anchoring on the CdTe/NiO photocathode, an evident increase in cathodic photocurrent could be noticed compared with pure pDNA anchoring (curve d), which indicated the formation of exciton–plasmon coupling between the CdTe QDs and AuNPs labeling. Incidentally, the characterization of the AuNPs-pDNA conjugates was rendered in Fig. S3. After MEA blocking, the cathodic photocurrent decreased mildly (curve e) owning to weak charge-transfer ability of this small organic molecule. While the sensing electrode was incubated with tDNA, the cathodic photocurrent decreased greatly (curve f), demonstrating that the tDNA hybridization induced occurrence of disappeared exciton–plasmon coupling and generated exciton energy transfer had successful happened. The expected variation trend of the photocurrent response hence confirmed successful building of the cathodic DNA bioassay.

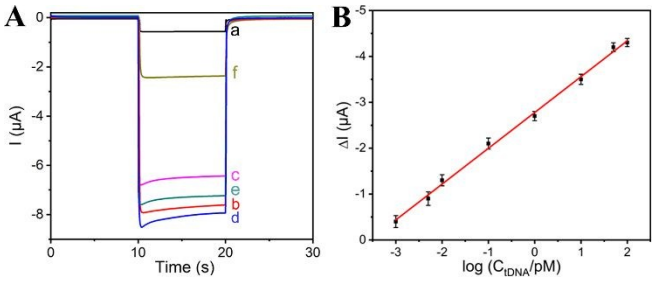

Fig. 3. (A) Photocurrent responses of (a) the NiO cathodic substrate, (b) after CdTe QDs modification, (c) after pure pDNA anchoring or (d) after AuNPs-pDNA conjugates anchoring, (e) after MEA blocking, and (f) after incubation with 1 μM tDNA. (B) calibration curve of the cathodic PEC biosensor toward different concentrations of tDNA from 1 fM to 100 pM. $\Delta I=I_0-I$, I_0 and I stand for photocurrent responses of the DNA sensor before (I_0) and after (I) tDNA hybridization.

Furthermore, the optical imaging was utilized to visually monitor and verify the final production of the energy transfer on the sensing electrode, as shown in Fig. S4. In the absence of tDNA, the pDNA was in hairpin shape and the labeled AuNPs were in close contact with CdTe QDs. In this case, as shown in Fig. S4A, the fluorescence quenching happened due to Förster

resonance energy transfer (FRET).[22,23] Once the occurrence of the DNA hybridization, the pDNA changed from hairpin shape into a rigid rod-like double helix, and the AuNPs labels left from the electrode surface, keeping a certain distance with the CdTe QDs on the sensor surface. At this time, as exhibited in Fig. S4B, a fluorescence recovery was clearly observed owning to the inhibited FRET.[24,25] Thus, optical imaging offered a visual evidence in realizing the DNA biosensor design.

The tDNA detection was operated upon the distance-induced signal on-off mechanism controlled by AuNPs labeling. Under optimal condition (Fig. S5), the analytical performance of the cathodic PEC biosensor was evaluated. As revealed in Fig. 3B, in the scope of 1 fM to 100 pM, the photocurrent signal weakened linearly with increase in the logarithm of tDNA concentration. The regression equation was $\Delta I = -2.76 - 0.78 \log C$ (pM) with the correlation coefficient of 0.997, and the limit of detection (LOD, S/N=3) was acquired to be 0.28 fM, which was lower than or comparable to previously reported DNA biosensor for tDNA detection.[26-30] The selectivity of the cathodic PEC biosensor was depicted in Fig. S6, and the result verified that the photocurrent signal was specifically triggered by the tDNA hybridization with pDNA. The stability and repeatability of the PEC biosensor were also studied (see the ESI file), and the results of high stability and acceptable reproducibility were acquired. The feasibility of the cathodic PEC biosensor was examined by detecting PCR products of practical samples. K562 cell and negative real sample were ordered as the targets. As depicted in Fig. S8, the photocurrent response of the cathodic PEC biosensor to PCR products from K562 cell showed an evident decrease, while the photocurrent response to negative real sample was nearly the same as the blank control. The results thus confirmed a promising application potential of the designed PEC biosensor.

In summary, an advanced signaling on-off mechanism controlled by plasmonic AuNPs was first demonstrated to build a powerful photocathodic DNA bioanalysis. The 3D structured CdTe/NiO photocathode had an evident cathodic photocurrent, being qualified for the PEC matrix. The different roles of plasmonic AuNPs labeling were triggered by conformation change of pDNA from hairpin structure to rigid rod-like double helix upon hybridizing with tDNA. Before tDNA hybridization, the formation of exciton–plasmon coupling between the CdTe QDs and plasmonic AuNPs could evidently enhance the cathodic photocurrent (signal on). After tDNA hybridization, the disappearance of exciton–plasmon coupling concurrent with the generation of exciton energy transfer conspicuously decreased the cathodic photocurrent (signal-off). Benefiting from this simple but superior signaling on-off mechanism, the photocathodic DNA bioanalysis offered an ultralow LOD and excellent selectivity for the detection of model tDNA of BCR/ABL fusion gene. More generally, we believe that the ingenious work especially in superior signaling mechanism would stimulate more inspiration to explore other various powerful cathodic PEC bioassays.

This work is supported by the Project Fund for Shangdong Key R&D Program (2019GSF108175), and the National Natural Science Foundation of China (21603099).

Conflicts of interest

View Article Online
DOI: 10.1039/C9CC08472J

There are no conflicts to declare.

Notes and references

1 W. Zhou, L. Hu, L. Ying, Z. Zhao, P. K. Chu, X. F. Yu, *Nat. Commun.*, 2018, **9**, 5012.
2 R. Yamashige, M. Kimoto, R. Okumura, I. Hirao, *J. Am. Chem. Soc.*, 2018, **140**, 14038−14041.
3 W. W. Zhao, J. J. Xu, H. Y. *Chen, Chem. Rev.*, 2014, **114**, 7421–7441.
4 Y. Zheng, W. Liang, Y. Yuan, C. Xiong, S. Xie, H. Wang, Y. Chai, R. Yuan, *Biosens. Bioelectron.*, 2016, **81**, 423–430.
5 Y. Chu, A. P. Deng, W. J. Wang, J. J. Zhu, *Anal. Chem.*, 2019, **91**, 3619−3627.
6 Z. Song, G. C. Fan, Z. Li, F. Gao, X. Luo, *Anal. Chem.*, 2018, **90**, 10681−10687.
7 H. Wang, B. Zhang, F. Zhao, B. Zeng, *ACS Appl. Mater. Interfaces*, 2018, **10**, 35281−35288.
8 Y. Zhu, K. Yan; Z. Xu, J. Wu, J. Zhang, *Biosens. Bioelectron.*, 2019, **131**, 79–87.
9 W. X. Dai, L. Zhang, W. W. Zhao, X. D. Yu, J. J. Xu, H. Y. Chen, *Anal. Chem.*, 2017, **89**, 8070−8078.
10 G. C. Fan, H. Zhu, Q. Shen, L. Han, M. Zhao, J. R. Zhang, J. J. Zhu, Chem. Commun., 2015, 51, 7023–7026.
11 X. M. Shi, L. P. Mei, Q. Wang,; W. W. Zhao, J. J. Xu, H. Y. Chen, *Anal. Chem.*, 2018, **90**, 4277−4281.
12 C. Strelow, T. S. Theuerholz, C. Schmidtke, M. Richter, J. P. Merkl, H. Kloust, Z. Ye, H. Weller, T. F. Heinz, A. Knorr, H. Lange, *Nano Lett.*, 2016, **16**, 4811−4818.
13 S. K. Dutta, S. K. Mehetor, N. Pradhan, *J. Phys. Chem. Lett.*, 2015, **6**, 936−944.
14 B. K. Patra, S. Khilari, D. Pradhan, N. Pradhan, *Chem. Mater.*, 2016, **28**, 4358–4366.
15 X. Yu, A. Shavel, X. An, Z. Luo, M. Ibanez, A. Cabot, *J. Am. Chem. Soc.*, 2014, **136**, 9236−9239.
16 F. Odobel, L. L. Pleux, Y. Pellegrin, E. Blart, *Acc. Chem. Res.*, 2010, **43**, 1063–1071.
17 Y. Q. Zhang, X. H. Xia, J. P. Tu, Y. J. Mai, S. J. Shi, X. L. Wang, C. D. Gu, *J. Power Sources*, 2012, **199**, 413–417.
18 J. H. Bang, P. V. Kamat, *ACS Nano*, 2009, **3**, 1467–1476.
19 T. Lin, F. Huang, J. Liang, Y. Wang, *Energy Environ. Sci.*, 2011, **4**, 862−465.
20 A. O. Govorov, G. W. Bryant, W. Zhang, T. Skeini, J. Lee, N. A. Kotov, J. M. Slocik, R. R. Naik, *Nano Lett.*, 2006, **6**, 984–994.
21 W. W. Zhao, J. Wang, J. J. Xu, H. Y. Chen, *Chem. Commun.*, 2011, **47**, 10990–10992.
22 T. Neumann, M. L. Johansson, J. D. Kambhampati, W. Knoll, *Adv. Funct. Mater.*, 2002, **12**, 575–586.
23 D. J. Maxwell, J. R. Taylor, S. Nie, *J. Am. Chem. Soc.*, 2002, **124**, 9606–9612.
24 M. Stanisavljevic, S. Krizkova, M. Vaculovicova, Rene Kizek, V. Adam. *Biosens. Bioelectron.*, 2015, **74**, 562–574.
25 Y. Wang, D. Gao, P. Zhang, P. Gong, C. Chen, G. Gao, L. Cai. *Chem. Commun.*, 2014, **50**, 811–813.
26 H. Wu, X. Zhou W., Cheng, T. Yuan, M. Zhao, X. Duan, S. Ding, *Analyst*, 2018, **143**, 4974–4980.
27 X. M. Shi, G. C. Fan, Q. Shen, J. J. Zhu, *Appl. Mater. Interfaces*, 2016, **8**, 35091–35098.
28 C. Tao, Y. Yan, H. Xiang, D. Zhu, W. Cheng, H. Ju, S. Ding, *Chem. Commun.*, 2015, **51**, 4220–4222.
29 Y. Xu, X. Bian, Y. Sang, Y. Li, D. Li, W. Cheng, Y. Yin, H. Ju, S. Ding, *Sci. Rep.*, 2016, **6**, 32370.
30 L. Wang, E. Hua, M. Liang, C. Ma, Z. Liu, S. Sheng, M. Liu G. Xie, W. Feng, *Biosens. Bioelectron.*, 2014, **51**, 201–207.